The solvation dynamics of CO2 by Quantum Mechanical Molecular Dynamics

Article *in* Chemical Physics Letters · October 2023

DOI: 10.1016/j.cplett.2023.140861

CITATIONS
0

READS
61

3 authors:

Md Al Mamunur Rashid
Korea Institute of Science and Technology
24 PUBLICATIONS **127** CITATIONS
SEE PROFILE

Thamina Acter
East West University (Bangladesh)
31 PUBLICATIONS **488** CITATIONS
SEE PROFILE

Nizam Uddin
Daffodil International University
53 PUBLICATIONS **1,189** CITATIONS
SEE PROFILE

PCCP

ROYAL SOCIETY OF CHEMISTRY

PAPER

View Article Online
View Journal | View Issue

Cite this: *Phys. Chem. Chem. Phys.*, 2023, **25**, 31194

Identifying the acidic or basic behavior of surface water: a QM/MM-MD study

Md Al Mamunur Rashid, [a] Mofizur Rahman,[b] Thamina Acter[c] and Nizam Uddin*[d]

Received 7th May 2023,
Accepted 1st November 2023

DOI: 10.1039/d3cp02080k

rsc.li/pccp

Controversies on the water surface were theoretically addressed with the help of large scale quantum mechanical molecular dynamics (QMMD) simulations on water surface model systems with and without excess hydroniums and hydroxides. It was revealed that the thermodynamic surface structures of these ions strongly depend on their location and dipole orientation. Fast hydronium diffusion by proton transfer establishes a wider kinetic depth distribution (~6 Å) than that predicted by its thermodynamic affinity for the water surface, while slow hydroxide is shallowly trapped below the outermost molecular layer (3–4 Å). In addition, the anisotropic orientation of surface water dipole can generate a substantial magnitude of surface potential, which extends to a depth of a few molecular layers. With these distinctively different surface properties of two ions and water molecules, the seemingly contradictory observations of acidic and negatively charged water surfaces may be successfully explained. That is, the negative surface charge of neutral water mostly stems from intrinsic water properties such as water dipole orientation and electron density spillage at the surface, rather than surface OH^- ions. The enhanced acidity of the water surface can be attributed in large part to the kinetic depth profile of ion density in addition to static thermodynamic origin. Furthermore, the different depth profiles of the two ions may differently affect the surface-sensitive spectroscopic observations.

1. Introduction

The water surface is an important subject of research in many scientific disciplines and technologies. Despite extensive studies to understand the properties of the water surface at a molecular level, many mysteries and controversies still remain. The origin of the surface charge of water is one example.[1] Electrophoretic mobility measurements of air bubbles and oil drops in water showed that the surface of neutral water is negatively charged, with the zeta (ζ) potential of a bubble in neutral pure water of about −65 mV.[2,3] The observations were interpreted as evidence of the strong adsorption of hydroxide (OH^-) ions at the water surface.[3] On the other hand, nonlinear optical spectroscopic studies of the structure of air/water interfaces[4,5] and interfacial acid–base reactions[6] indicated that hydronium (H^+) ions have a higher concentration at the surface of water than in the bulk phase. In the case of OH^- ions, nonlinear spectroscopic studies reported results that can be interpreted in terms of a wide range of behaviors,[4,5] from slight enhancement of OH^- at the air/water interface to strong depletion, but not strong enhancement.

Computational studies have not yet reached a consensus in this issue either. A majority of MD simulations with CP2K/BLYP/DZVP,[7] POL3,[8] CPMD/BLYP,[9] MS-EVB3,[10] and SWM4-NDP[11] show that H^+ ions are attracted to the air–water interface,[7–11] but OH^- ions do not display preference for the surface.[7,8,11] Contrasting to these results, other theoretical studies with polarizable models,[12] CP2K/BLYP/TZV2P,[13,14] and polarizable MS-EVB[15] indicate that H^+ ions have equal propensity for the surface and bulk, whereas OH^- ions exhibit a shallow minimum at the interface. It appears that, even with the same AIMD (*ab initio* molecular dynamics) simulation techniques, contrasting conclusions have been deduced.

The orientation of surface water dipoles can also contribute to the surface charge and potential. The surface potential resulting from water dipoles has been examined using molecular dynamics simulations using different water models and *ab initio* charge distributions.[16–26] However, the surface potentials predicted from these simulations showed a large variation; the surface potentials calculated from the *ab initio* charge distributions have positive values ($\chi \approx +3.1$ V; negative surface charges with the O atom of surface water pointing outward),[22,23] whereas several point-charged water models give negative values

[a] *Clean Energy Research Center, Korea Institute of Science and Technology, Seoul, 02792, South Korea*
[b] *Research and Development Center, Berger Paints Bangladesh Limited, Berger House, Dhaka-1230, Bangladesh*
[c] *Department of Mathematical and Physical Sciences, East West University, Aftabnagar, Dhaka-1212, Bangladesh*
[d] *Department of Nutrition and Food Engineering, Daffodil International University, Birulia, Dhaka-1216, Bangladesh. E-mail: nizamu.nfe@diu.edu.bd; Fax: +8802224441835; Tel: +8802224441833, ext. 34100*

($\chi \approx -0.9$ to -0.5 V).[24–26] Recently, Cendagorta and Ichiye[21] suggested that the discrepancy may have originated from the inclusion of multipole moments of the charge distribution in the calculation of the electrostatic potential, which could be a source of an error, and that the surface potential can be obtained mostly by considering only the dipole orientation of water in MD simulations. In a recent study conducted by G. Cassone,[27] the profound impact of electric fields on water molecules was explored, with a particular focus on the proton transfer process and the role of nuclear quantum effects (NQEs). Through the use of computer simulations and *ab initio* molecular dynamics, this research delved into the formation of charged species, such as H^+ and Zundel ions, under the influence of electric fields. The inclusion of NQEs was found to be a pivotal factor, significantly altering proton conductivity and water behavior.[28–30] The study underscores the crucial importance of considering NQEs when investigating the behavior of light atoms, particularly protons, in the presence of electrostatic gradients. NQEs were revealed to reduce the molecular ionization threshold and transform water into a protonic semiconductor, increasing proton conductivity by approximately 50%. Furthermore, the quantum nature of protons, encompassing zero-point motion and quantum tunneling, exerts a profound influence on proton transfer properties under electric fields. Thus, incorporating the NQEs in simulations is indispensable for capturing the complete spectrum of proton transfer behavior and providing an accurate description of water's response to electrostatic gradients.

An important question in the discussion of the surface charge of water is the thickness of the surface phase. This issue has been somewhat neglected in previous studies of water surface properties, although it is a long-standing question in the use of the Gibbs adsorption equation to relate the surface free energy change to the surface composition. The original Gibbs formulation assumed zero thickness for the surface phase. In reality, however, chemical composition at a surface changes gradually from the outermost layer to the interior region. Therefore, it is important to know how the properties of interest vary across the surface region, or adequately define the thickness of the corresponding surface phases, the region in which the properties can be differentiated from those in the bulk phase. The surface phase thickness is particularly important in the discussion of various experimental observations on the surface charge issue because different techniques probe different depths of a surface. Key questions here include the distributions of H^+ and OH^- ions near the water surface and water dipole orientations.

Several years ago, Lee *et al.*[31] examined the depth distributions of H^+ and OH^- ions at the surface of amorphous solid water (ASW) samples by measuring the surface voltage produced by an ionized acid or base. While both H^+ and OH^- ions showed tendency to reside on the surface, the former was distributed over a deeper region from the surface than the latter, and this difference resulted in a different voltage of the acid or base-added surface. This observation reveals that it is necessary to account for the depth distributions of H^+ and OH^- ions in order to properly understand the surface chemical and electrical properties resulting from these ions.

In the present paper, we explore some fundamental questions related to the surface charge issue of water using a series of quantum mechanical (QM) molecular dynamics (MD) simulations. We used the hybrid QM/MM method with advanced water models, which has been shown[32] to be successfully applied to MD simulations of various chemical processes in aqueous solutions.[33–42] Specific questions explored in this work include the propensities of H^+ and OH^- ions for the water surface, their depth distributions and dynamic properties, the orientation of water dipoles, and their contribution to the surface potential and charge. We also speculate how these fundamental surface phenomena may be able to explain some of the disputable experimental observations reported in the literature.

2. Computational methods

A QM/MM water slab model of a 30 × 30 × 30 Å box was designed for the surface dynamics of H_3O^+ and OH^- ions as shown in Fig. 1. It includes a total of 900 water molecules with a liquid density of 1.012 g cm^{-3}. A cylindrical QM region containing either H_3O^+ or OH^- with 35 QM water molecules was embedded as represented with green color. The height and

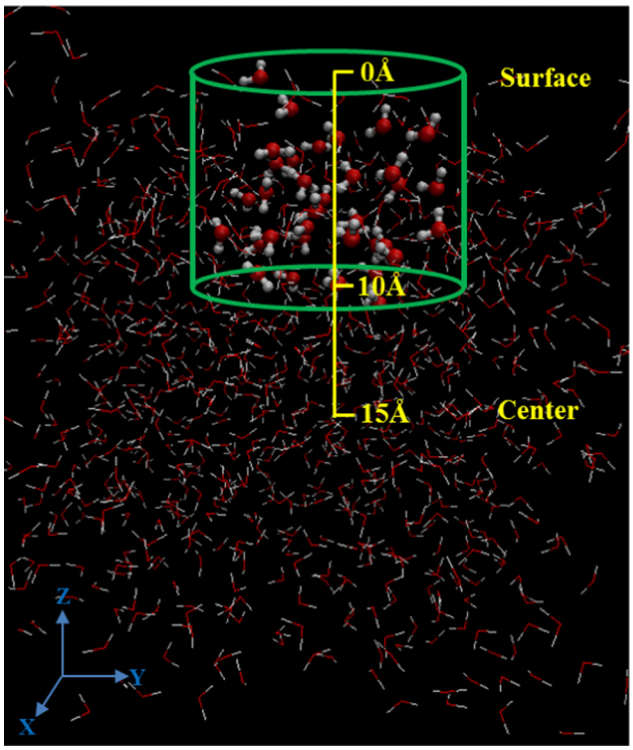

Fig. 1 A water slab model of the 30 × 30 × 30 Å box. In order to model the air/water interfaces, the periodic length along the z-direction was set to 100 Å. The cylindrical QM boundary condition with the height and radius of 10 Å and 6 Å, respectively, is applied on the center of the surface as indicated with a green line. The depth of water is measured from the air/water interface. Therefore, the center of the box along the z-direction is 15 Å as shown above. More detailed descriptions of models are explained in the computational details.

radius of the cylindrical boundary were 10 Å and 6 Å, respectively. In order to model the vacuum/water interfaces, the periodic length along the *z*-direction was set to 100 Å. To prevent the mixing between QM and MM waters, the harmonic force constant of 2 kcal mol^{-1} $Å^{-2}$ was applied at the boundary of the cylinder. The center of mass of the QM molecule was also constrained to remain in the center of the cylinder with a force constant of 5.0 kcal mol^{-1} $Å^{-2}$.

In our previous study,[42] we conducted QM/MM-MD simulations to assess proton transfer efficiency using various quantum chemical methods, including DFT with various functionals such as BLYP and B3LYP, as well as MP2 and CCSD(t). We also explored various basis sets, including 6-31G(d), cc-pVDZ, cc-pVTZ, and cc-pVQZ. Our findings from these investigations led to the conclusion that B3LYP and MP2 represented appropriate levels of theory to accurately describe both hydronium transport and hydroxide transport. We concur that a double-zeta basis set like 6-31G(d) may be viewed as relatively small for DFT and might not provide highly accurate results for systems characterized by significant electron correlation. Typically, basis set convergence is expected at the triple-zeta level for such systems. However, we have found that 6-31G(d) consistently delivers excellent results while remaining cost-effective and efficient, aligning well with experimental data.[32–42] The use of a triple-zeta basis set in QM/MM-MD simulations would substantially increase computational demands, including time and cost, while offering only marginal improvements in accuracy.

MD simulations with the *NVT* ensemble were performed at two different temperatures of 250 K and 300 K, where the former condition possibly represents ASW. To describe the MM waters, the TIP5P water model was carefully selected after confirming the minor effect of solvent polarization as a result of the preliminary simulations. In order to obtain the equilibrium properties of H_3O^+ and OH^- ions along the *z*-direction (depth of water), umbrella samplings (US) were performed with a force constant of 10 kcal mol^{-1} $Å^{-2}$. The choice of these force constants (2, 5, and 10 kcal mol^{-1} $Å^{-2}$) was made after extensive testing to ensure that they do not disrupt the simulated water behavior. A total of seven windows along the *z* direction were utilized which covers z = 0 Å (surface) to z = 6 Å (bulk) depth with a spacing of 1.0 Å. At each umbrella window, QM/TIP5P-MD was performed for 50 ps with initial equilibrations of 10 ps. The potentials of mean force (PMF) from the umbrella samplings were obtained using the weighted histogram analysis method (WHAM).[43] The two-dimensional PMF was obtained by simply binning the dipole A_D angle on the basis of one-dimensional umbrella sampling windows along the depth coordinate, R_z = 0–6 Å. Our simulations produced smooth and noiseless PMF profiles (see Fig. 2 and 3) covering a range from 0 to 6 Å (bulk) depth with a spacing of 1.0 Å, indicating that the selected force constants do not adversely affect the behavior of the simulated water molecules. Furthermore, we estimated the statistical error of our simulations by calculating the square of cumulative statistical error, following the method suggested by Zhu and Hummer.[44] The resulting estimated square of cumulative error in our calculated free energy is

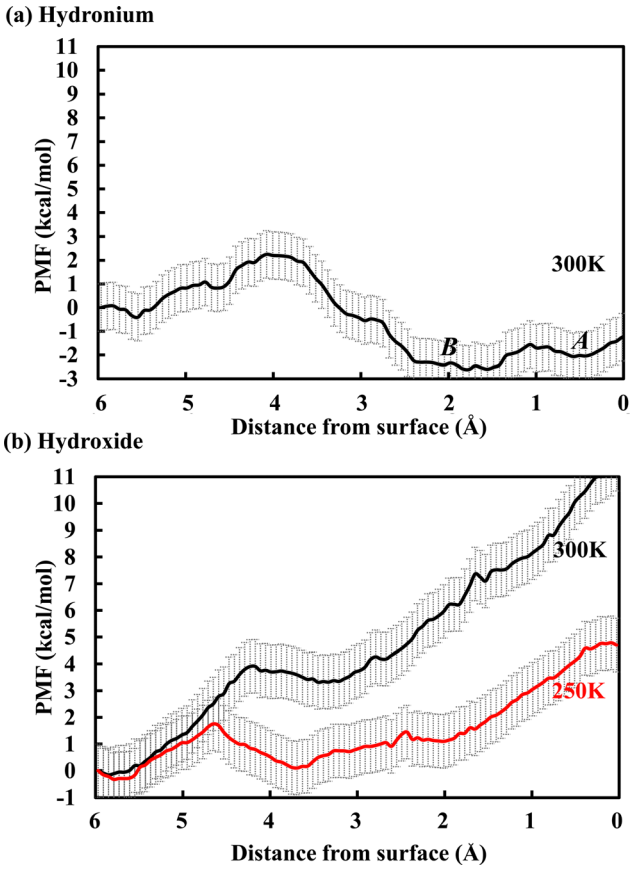

Fig. 2 Potentials of mean force (PMF) along the R_z-coordinate perpendicular to the interface for (a) H_3O^+ at 300 K and (b) OH^- at 300 K and 250 K. Error bars are shown as the vertical dashed lines throughout the graph.

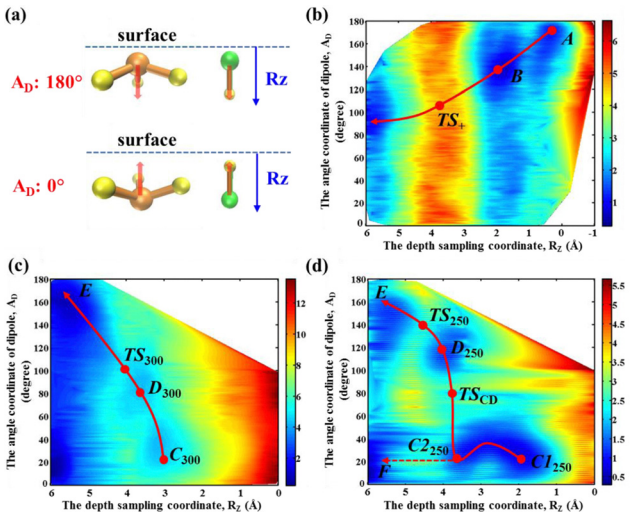

Fig. 3 (a) Definitions of R_z and A_D. The angle 180° indicates that oxygen of hydronium or hydroxide points to the bulk, and angle 0° is toward the surface. 2D PMFs along the R_z-coordinate and rotational angle between the *z*-direction and the dipole (A_D) of (b) hydronium at 300 K and that of hydroxide at (c) 300 K and (d) 250 K were obtained on the basis of one-dimensional umbrella sampling windows.

0.10 kcal mol^{-1}, which indicates that our PMF calculations have reached convergence.

Using the same water slab model, we also performed MD simulations for the water dipole orientation at the water surface with non-polarizable TIP5P as well as polarizable EFP (Effective Fragment Potential) parameters. While alternative high-end water potentials such as MBpol and q-aqua exist, we chose the QM/MM-EFP approach due to several advantages: (i) it significantly reduces computational overhead, (ii) it offers high computational accuracy, and (iii) it allows for improvement by combining advanced quantum chemical theories with traditional atom-center Gaussian basis sets. It should be noted that we did not take into account any dispersion correction in our study during the MD calculation, as we have already proved that our QM/MM-MD approach can yield the similar results without considering the dispersion correction.[32–42] MD simulations with these parameters ran for 1 ns with initial equilibrations of 100 ps within the *NVT* ensemble at a temperature of 300 K. The smooth and converged PMF, obtained from the MD simulations of 50 ps (with an initial equilibration of 10 ps) and 1 ns (with an initial equilibration of 100 ps), ensured us that the simulation time was accurate. All calculations were performed with a modified version of GAMESS.[45]

3. Results and discussion

3.1. Free energy and structure of surface-residing H^+ and OH^- ions

To explore the propensity of hydronium and hydroxide ions for the water surface, their free energy surfaces were calculated along the penetration depth. To obtain the corresponding PMF (potential of mean force), umbrella samplings of the two ion positions along the *z*-direction (depth, R_z) were individually performed within the QM region of our embedded QM/MM model systems as discussed in the computational details. Since the umbrella samplings of ion positions were performed at R_z = 0–6 Å, the PMFs would represent the ion position at the water surface as well as the early stage of penetration into the bulk region (see Fig. 2). In the case of hydronium simulations (Fig. 2a), a strong minimum appears at R_z = 0–2 Å, which is below the free energy of the reference point (R_z = 6 Å) by 2 kcal mol^{-1}. This surface preference of hydronium is consistent with previous theoretical studies[7–11] as well as with experiments.[4–6] However, in contrast to previous theoretical studies, two minima near R_z = 0.5 and 2.0 Å appear in our hydronium PMF. We have also computed error bars for the PMF using umbrella sampling simulations. The error bars were calculated following best practices, and we found that they are within an acceptable range.

To characterize the minima, two-dimensional PMF was generated by adopting an additional coordinate of hydronium dipole angle (A_D, see Fig. 3a) in addition to R_z, as shown in Fig. 3b. Remarkable angle (A_D) dependencies can be found in the two-dimensional PMFs. Two minima appear at R_z = 2.0 Å in Fig. 3b, a deep one at A_D = 140° and a shallow one at A_D = 20–80°. The former (*A*) corresponds to a hydronium structure with an oxygen dangling bond. The dangling bond is a bond without a hydrogen bond due to it pointing to the gas phase. On the other hand, the latter represents a hydronium with a hydrogen dangling bond. Near the top-most layer (R_z = 0.5 Å), a minimum (*B*) with A_D = 140°–180° is found, which represents a strong preference of the hydronium structure with an oxygen dangling bond. The distance of ~1.5 Å between *B* and *A* may correspond to the intra-layer O–O vertical distance within a water bilayer, implying a remarkable vestige of the water bilayer at the aqueous water surface involving a hydronium ion. This result is quite reasonable, since the water surface should be structurally much more constrained than bulk due to the lack of the surrounding water molecules. Therefore, the two minima around R_z = 0–2 Å in Fig. 2a is in fact composed of A and B types, representing a water bilayer structure. A free energy barrier at R_z = 4 Å (Fig. 2a) separates the surface bilayer and bulk regions. Fig. 3b shows that the barrier region (TS_+) has slight preference at a dipole angle of ~100°. Collectively, the hydronium penetration path into the bulk region can be depicted as a sequence of A → B → TS_+, which accompanies dipole angle change from 180° to 100° during the event.

Fig. 2b shows the results of QM/MM-MD simulations for hydroxide at 250 and 300 K. Two different temperatures were chosen for the simulation because the hydroxide diffusion mechanism depends strongly on temperature, from predominant Brownian diffusion at low temperature to proton transfer at high temperature.[42,46] Our simulation at 300 K yields only a weak minimum near R_z = 3.5 Å in Fig. 2b, in accord with previous studies,[8,11] showing that the surface preference of hydroxide is weaker than that of hydronium. However, the situation changes quite significantly in the low temperature simulation, where the minimum becomes almost as stable as the reference point.

The respective two-dimensional PMFs are presented in Fig. 3c and d. Two weak minima at D_{300} (3.7 Å, 80°) and C_{300} (3.0 Å, 20°) appear in the 2D PMF at 300 K of Fig. 3c. They correspond to the structures where the hydroxides are nearly parallel and perpendicular to the surface, respectively (see the notation in Fig. 3a). The former (D_{300}) may represent an intermediate between the surface and bulk structures, while the latter (C_{300}) corresponds to the hydrogen dangling bond structure of hydroxide. The C_{300} structure can be understood by the fact that the hydroxide hydrogen is much less positively charged than hydronium and neutral water,[47] which does not favorably interact with solvent water. A low free energy barrier (TS_{300}) connecting D_{300} with the bulk region exists at (100°, 4.0 Å). Collectively, the bulk penetration of hydroxide can be described as a sequence of C_{300} → D_{300} → TS_{300} with the corresponding 20° to 160° angle rotation. The large angle change indicates the importance of rotational dynamics for the penetration. As discussed above, since the proton transfer plays a minor role in the hydroxide diffusion, the depth distribution of hydroxide can be mostly determined by the slow rotation and translation dynamics of molecular hydroxide. The slow rotation and translation dynamics can be largely affected by the temperature, which is demonstrated by the

PMF simulated at 250 K (Fig. 2b). As compared to 300 K, the overall free energy surfaces are significantly lowered in the simulation at 250 K. According to the 2D PMF of Fig. 3d, the location of hydroxide with a hydrogen dangling bond is broadly distributed from 2.0 ($C1_{250}$) to 3.7 Å ($C2_{250}$), expanding its depth thickness. On the other hand, the D_{250} has a larger dipole angle of 120° as compared to D_{300}. These species (C and D) become significantly more stable at lower temperature. It is pointed out that both $C2_{250}$ and D_{250} coexist at approximately the same depth of 4.0 Å. A large rotational barrier (TS_{CD}) between the species $C2_{250}$ and D_{250} discourages their interconversions in the low temperature. Collectively, the rotational penetration of hydroxide at 250 K can be described as a sequence of $C1_{250} \rightarrow C2_{250} \rightarrow TS_{CD} \rightarrow D_{250} \rightarrow TS_{250}$. A translational diffusion can also occur directly *via* a sequence of $C2_{250} \rightarrow F$ with a barrier of $\sim$2 kcal mol^{-1}. In short, the surface preference of hydroxide is greatly enhanced at lower temperature, which can be attributed to the temperature sensitivity of rotational and translational dynamics as well as the broad depth distribution of hydroxide with a hydrogen dangling bond.

The snapshots of hydronium at A and B points, and hydroxide at $C1_{250}$, $C2_{250}$, D_{250}, and E are shown in Fig. 4. The bold orange line represents the surface, and the orange and green balls represent hydronium and hydroxide, respectively. The dotted yellow line represents the hydrogen bonds connected either with hydronium or hydroxide. Fig. 4a and b show the structures at A and B, respectively, where oxygen dangling bonds are clearly seen. Fig. 4c–f represent the rotational penetration sequence of hydroxide ($C1_{250} \rightarrow C2_{250} \rightarrow D_{250} \rightarrow E$), where the rotation of the dipole angle is clearly seen. Our analysis revealed the distinctly different structures of surface hydroniums and hydroxides, which strongly depend not only on the depth but also on their dipole angles. Hydroxide tends to reside 1–2 Å deeper than hydronium. Both surface ions prefer particular dipole angles, representing their restricted surface structures. In the case of the surface hydroxide structure, the surface preference is significantly increased at a lower temperature due to its slow Brownian dynamics. These differences in surface structures would yield an asymmetric distribution of the two ions near the surface.

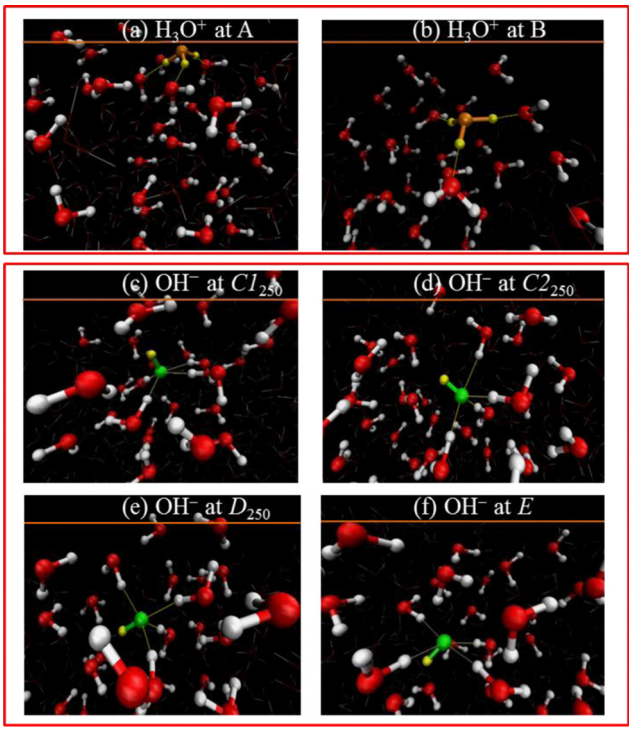

Fig. 4 Snapshots of the most probable configurations of hydronium at A (a) and B (b), and those of hydroxide at $C1_{250}$ (c), $C2_{250}$ (d), D_{250} (e) and E (f) along the z-direction.

However, the behavior of hydronium ions at different temperatures, especially in the context of proton transfer, is a complex interplay of various factors, including thermal fluctuations, quantum effects, and energetic barriers. At lower temperatures, the quantum nature of particles becomes more pronounced, leading to larger zero-point motion and an increased likelihood of quantum tunneling events. These quantum effects can indeed favor proton hopping mechanisms over classical Brownian motion, which relies on thermal fluctuations. In this study, we emphasized the fast proton hopping mechanism with a low energy barrier, although it should be acknowledged that this mechanism may involve quantum effects, particularly at lower temperatures. The preference for proton hopping could be due to a combination of thermal fluctuations and quantum effects, with quantum tunneling playing a more significant role at lower temperatures. It's crucial to recognize that estimating the exact contributions of these factors can be challenging due to the subtlety of the energy differences involved and the complexity of proton transfer in the condensed phase. Additionally, the dominance of one mechanism over the other may depend on the specific conditions and timescales of the system under study. Therefore, the discussion regarding the dominant proton transfer mechanism at different temperatures can be revisited to consider the interplay between thermal fluctuations and quantum effects, especially in the context of the very subtle energy barriers involved in proton transfer processes. Further research and more refined computational techniques may be necessary to provide a more comprehensive understanding of this complex behavior.

3.2. Transport dynamics of H^+ and OH^-.

Analysis of the individual trajectories of hydronium and hydroxide revealed drastically different transport mechanisms of hydronium and hydroxide ions toward the interior region. The main transport mechanism of hydronium is proton hopping, whereas that of hydroxide is rotational diffusion. Such a difference is reminiscent of their transport behaviors in the bulk solution phase discovered in our previous work.[42] Fig. 5 shows the schematic transport traces of hydronium and hydroxide. While the OH^- ion diffuses into the bulk by a slow rotational process, the H_3O^+ ion takes a fast proton hopping mechanism. The proton hopping barriers were investigated by calculating the single point energy as a function of the location

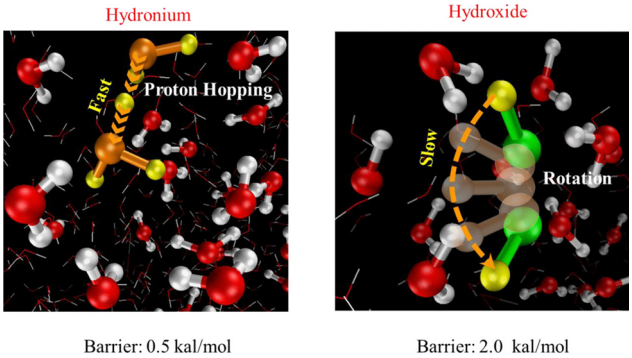

Fig. 5 The diffusion mechanisms from the surface to the bulk. While hydronium hops *via* proton transfer, hydroxide takes a slow rotational pathway.

of the proton transferring between the two O atoms. In the proton hopping mechanism, the H^+ of H_3O^+ is transferred to H_2O while the H^+ of H_2O is transferred to OH^-. The geometries of $H_5O_2^+$ and $H_3O_2^-$ at each location were first optimized at the B3LYP/6-31G(d) level of theory. By using B3LYP/6-31G(d), we can get the predicted hopping barrier which is closer to that of MP2,[42] indicating relatively small tunneling effects. In order to introduce the solvation effects into the hopping proton, the calculations were performed at O–O distances of 2.54 and 2.60 Å.[42] The shared proton was displaced along the line joining the two O atoms while keeping all other degrees of freedom fixed. While the proton hopping barrier is about 0.5 kcal mol^{-1},[42] the rotational free energy barrier is about 2.0 kcal mol^{-1} in Fig. 3d. The difference in barrier heights gives rise to different transport speeds of hydronium and hydroxide. In the solution phase, the typical timescale of proton transfer of hydronium is ~50 fs or less,[42] while that of hydroxide rotation dynamics is known to be 2.9 ps (295 K) and 9.2 ps (280 K).[48] Such a drastically different transport speed of two ions would yield quite different kinetic effects in their reaction behavior compared to that simply expected from their thermodynamic population distributions. This aspect shall be discussed in the following section.

3.3. Depth distributions of H^+ and OH^- ions: thermodynamic *versus* kinetic effect

The thickness of the surface phase, where the specific properties of interest are differentiated from those in the bulk, can be defined in terms of either the concentration profile of species (thermodynamic depth) or its acting range (kinetic depth). As described in the previous section, hydronium shows thermodynamic preference for surface residence and is distributed mainly at z = 0–2 Å. On the other hand, hydroxide is trapped in the region z = 3–4 Å, one bilayer below the surface.

The kinetic depth of hydronium may be estimated by considering the distance of proton transfer (PT) of surface-residing hydroniums. For this, the average rate of PT of hydroniums in the surface region (~4 Å) was calculated from the trajectories, and the results are shown in Table 1. The average PT rate for hydroniums at 300 K is 16.8 ps^{-1}, which indicates about 17 PT events for every 1 ps. In contrast, the average PT rate for hydroxide is 1.63 ps^{-1} at 300 K and 0.16 ps^{-1} at 250 K, which is 10–100 times slower than that for hydronium. In terms of transition state theory (TST), the free energy barrier differences between hydronium (0.5 kcal mol^{-1}) and hydroxide (2 kcal mol^{-1}) yielded a rate ratio of 2.3/0.12–10, which is consistent with our PT rate ratios from our simulations. Table 1 also shows the average PT distance in the z-direction. Utilizing these data, statistical ion distributions along the depth may be generated with the 1-D random-walk model of PT events. The ions initially residing at the surface develop a concentration profile as a function of z-distance and time, $c(z,t)$, which is calculated from the diffusion equation as

$$c(z,t) = \frac{n_0}{A(\pi D t)^{1/2}} e^{-z^2/4Dt},$$

where n_0 and A are the number of particles and surface area, respectively. The corresponding 1-D diffusion coefficient is $D = \varepsilon^2/2\delta t$, where ε is the size of a step of the random walk and δt is the time elapsed between two successive steps.

Table 1 The average proton transfer (PT) rate and PT distance for hydronium at 300 K, hydroxide at 300 K and hydroxide at 250 K at the outermost molecular layer (~4 Å)

	Avg. PT rate	Avg. PT z-distance
Hydronium (300 K)	16.8	1.03
Hydroxide (300 K)	1.63	1.28
Hydroxide (250 K)	0.16	1.04

Fig. 6 shows $c(z,t)$ for the hydronium at 300 K and hydroxide at 300 K and 250 K. These profiles indicate the kinetic depth distributions attained only by PT events at a specified time. The kinetic effect will extend the depth of the surface phase that is defined only by the static density profile of the ions. For instance, although hydronium mainly resides close to the surface in the thermodynamic distribution (Fig. 2), it can reach a depth of ~10 Å *via* proton transfer within 1 ps (Fig. 6a), thereby widening the effective thickness of the "acidic surface phase". Conversely, for an acid–base reaction occurring on the surface, subsurface hydroniums can traverse the surface region and participate in the surface reaction; this will increase the effective surface population of hydroniums from its actual surface population. On the other hand, this extra kinetic effect is relatively insignificant for hydroxide because of its inefficient PT event. In short, rapid proton transfer of hydroniums can make the effective thickness of the acidic surface phase significantly wider than the thermodynamic depth distribution of hydroniums.

3.4. Orientation of surface water dipoles

Apart from the contribution of surface residing ions, the surface potential of water can be produced by an inhomogeneous charge distribution at the surface. For example, at a metal surface the positive charge resides on the ions at lattice sites, while the electron density decays over a distance of ~1 Å from its bulk value to zero under vacuum. The surface potential due

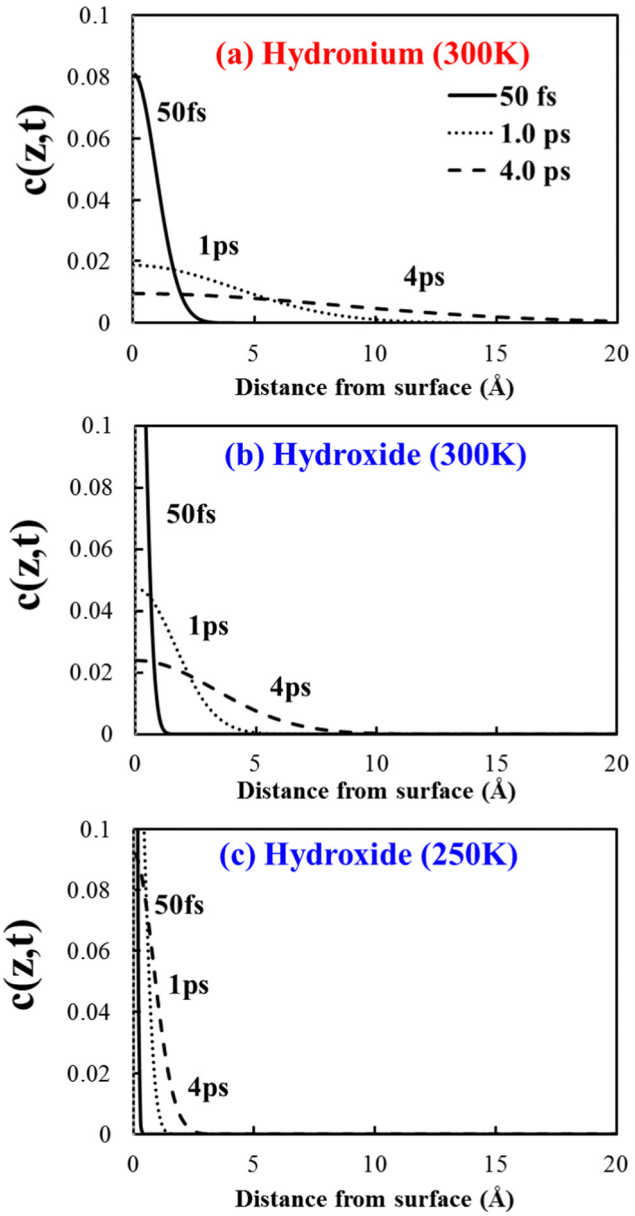

Fig. 6 The kinetic depth distributions of hydronium and hydroxide ions deduced from the analysis of ion penetration trajectories. The curves are for (a) hydronium at 300 K, (b) hydroxide at 300 K and (c) hydroxide at 250 K.

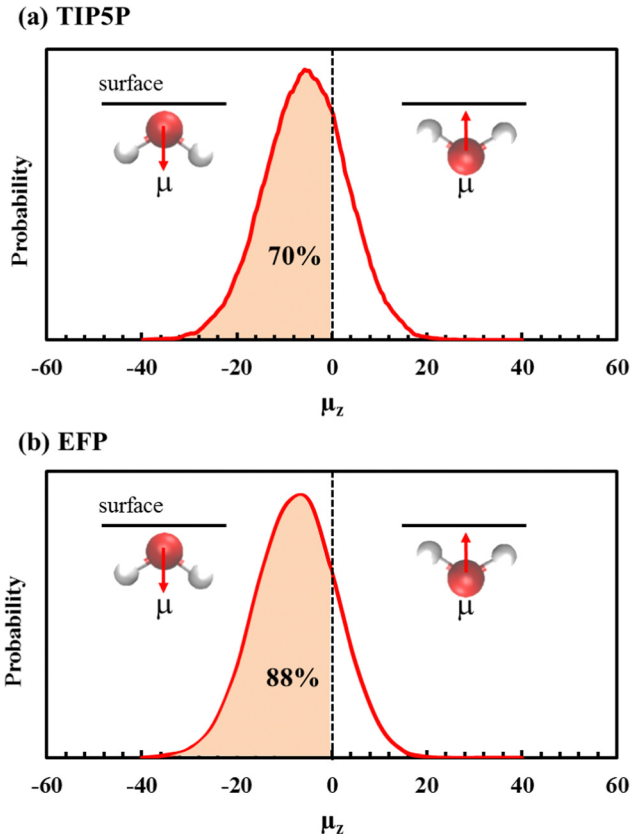

Fig. 7 The distributions of z-component dipole moment (μ_z) near the water surface (3 Å inside of the surface) obtained from MD simulations using (a) TIP5P and (b) EFP water potentials.

to the electron density spillage exists universally for all material surfaces and has a substantially large magnitude. At a water surface, anisotropic intermolecular interactions produce a small net orientation of water dipoles, and this can also give rise to a corresponding surface potential. In addition to the surface ions, water dipoles can create surface charges. We examined the orientation of water molecules near the water surface and estimated their contribution to the surface potential. As described in the Computational details section, MD simulations for the interfacial water structure were performed using both non-polarizable TIP5P and polarizable EFP water models. Since the EFP has not only polarization terms but also multipoles up to octupoles, it offers by far the most sophisticated molecular parameters and would properly represent the contributions of internal charge distribution to intermolecular electrostatic interactions. Fig. 7 displays the calculated orientational distribution of the z component of water dipoles in the first molecular layer (~3 Å depth). The negative value of μ_z in the figure indicates that the oxygen of water points outward, which corresponds to the negative surface charge. In the case of simulations with non-polarizable TIP5P, 70% of water molecules have configuration with negative dipole moment, whereas the simulations with EFP indicates 88%. Both water models consistently indicate the negative surface charge by the surface water dipole arrangements.

The surface potential originating from the orientation of surface water was estimated as follows. The surface potential is defined as the difference between the liquid-phase inner potential, $\varphi(z_{\text{inner}})$, and the vapor-phase outer potential, $\varphi(z_{\text{outer}})$. It may be calculated by integrating the total interfacial electric field, $E_z(z)$, across the air/liquid interface.

$$\begin{aligned}\chi &= \varphi(z_{\text{inner}}) - \varphi(z_{\text{outer}}) \\ &= -\int_{\text{outer}}^{\text{inner}} E_z(z')\mathrm{d}z' = -4\pi\int_{\text{outer}}^{\text{inner}} \rho(z')\mathrm{d}z' \end{aligned} \quad (1)$$

The interfacial electric field is obtained by integrating the spatial charge density at a distance z, $\rho(z)$, while the

contributions in x and y directions are averaged out by symmetry. The spatial charge density of each water molecule may be analyzed by a truncated multipole expansion including the terms from dipole and quadrupole. Recently, however, Cendagorta and Ichiye[21] have shown that the surface potential originates mostly from the contributions of dipole orientation, and the contributions of higher multipoles are insignificant. In this case, the surface potential is approximately calculated as:

$$\chi \approx -\int_{\text{outer}}^{\text{inner}} E_z(z')\mathrm{d}z' \approx -\int_{\text{outer}}^{\text{inner}} \frac{1}{\varepsilon_r \varepsilon_0} \sum_{i=1}^{N_A} \frac{\mu_{zi}}{A} \mathrm{d}z', \qquad (2)$$

where μ_z is the dipole moment along the z direction, A is the interface area in the x–y plane, and N_A represents the number of water molecules in the unit volume of $A \times 1$ ML (molecular layer). Fig. 8 represents the surface potential and corresponding interfacial electric field along the z direction as obtained by eqn (2) on the basis of the MD simulated structures of the water surface. The result from TIP5P-MD simulations yields a surface potential of χ = +0.56 V. This value is slightly higher than the surface potentials estimated in previous studies using different water models of TIP3P (+0.275 V), TIP4P-Ew (+0.4 V), TIP5P-E (+0.125 V), and SSDQO1 (+0.02 V).[21] The simulation with EFP yielded a surface potential of χ = +1.05 V, which is about twice higher than that from the non-polarizable TIP5P water model. The large variation in χ values indicates that the interfacial water structure and the resultant anisotropy in dipole orientation are very sensitive to the water models used.[21] Despite the large variance in magnitude, all the water models including sophisticated EFP indicate positive χ values, which unanimously support dipolar polarization at the water surface with the O atom pointing outward yielding the negative charge of the water surface.

We may define the surface region with anisotropic water dipole orientation as the ''dipolar surface phase'', where a strong internal electric field and a potential drop occur. The dipolar surface phase extends to a depth of ~10 Å for pure water, as shown in Fig. 8.

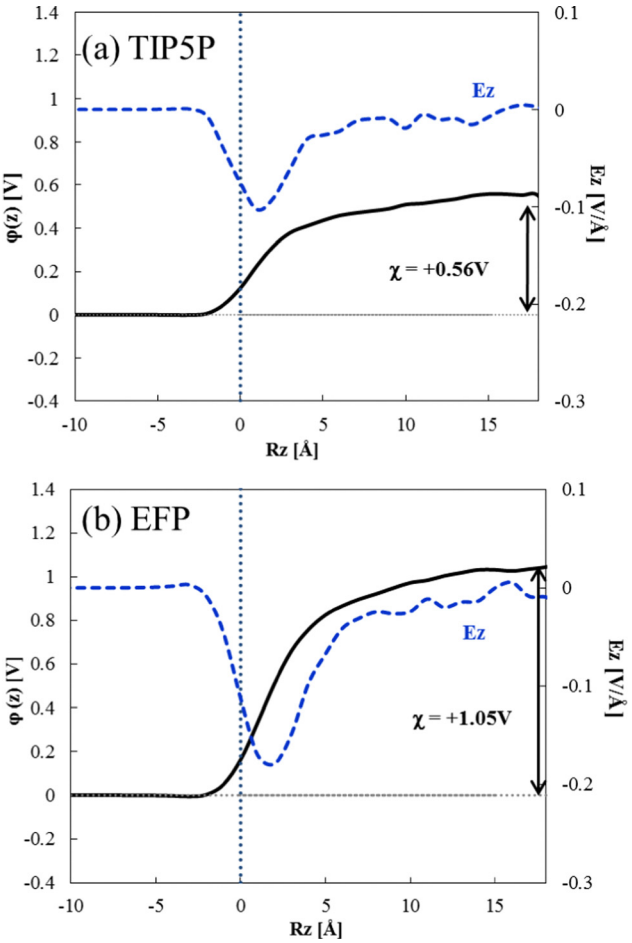

Fig. 8 The potential ($\varphi(z)$, left ordinate, solid line) and the electric field ($E_z(z)$, right ordinate, dashed line) along the z direction of the air/liquid interface obtained from the MD simulations using (a) TIP5P and (b) EFP potentials. The vertical dotted lines at z = 0 represents the surface with a density of 0.5 g cm^{-3}. A positive χ value means a negatively charged surface.

3.5. Rationale for different experimental observations

As mentioned in the Introduction, the experimental observations and theoretical interpretations show considerable discrepancies with regard to the charge state and acid–base properties of water surfaces. We may seek for a plausible explanation for some of the controversial issues on the basis of the depth distributions of hydronium and hydroxide ions and the dipolar surface phase of water described above.

(i) Surface charge of water. The surface of neutral water is negatively charged according to the measurements of ζ-potentials (about −0.1 V) of air bubbles and oil droplets in water[2,3] and streaming potentials of inert solids in contact with water. Our calculations show that a substantial magnitude of surface potential (χ = +0.56 V for the TIP5P model and 1.05 V for the EFP model) is developed by the anisotropic orientation of water dipoles at the surface, generating a dipolar surface phase with the negative pole at the surface. The dipolar phase extends to a depth of about 1 nm from the surface (Fig. 8). This depth is comparable to the location of the shear plane in electrophoretic mobility experiments, which is estimated to be usually between 0.3 and 6 nm from the dividing surface, depending on the nature of the interface.[49] Therefore, the voltage across the dipolar surface phase within the depth of the shear plane will contribute to the ζ-potential of the interface in electrophoretic experiments. We stress that the surface potentials calculated in the present work by MD simulations are qualitative and further improvement will be needed. Also, the location of the shear plane that divides the surface potential is quite uncertain. Nonetheless, the present calculations clearly show that the surface potentials originating from oriented water dipoles are large enough to account for the experimentally observed surface potentials of water, without the necessity of invoking the contributions from other sources such as externally added ions.

The accumulation of OH^- ions at the water surface might be considered as an alternative explanation for the negative charge of the water surface. Order-of-magnitude calculation shows that

to generate a surface voltage of ~0.1 V across a depth of ~1 nm, the ion density in the surface region needs to be as large as $\sim 5 \times 10^{17}$ ions per m^2. This would require an increase of the surface density of OH^- by 10^5 times compared to the OH^- concentration in the bulk phase of neutral (pH = 7) water. Such a high propensity of OH^- for the surface is unrealistic; neither experiments nor theoretical models support the strong adsorption of OH^- at the water surface. There seems to be only one report that claims strong interfacial charging of oil-in-water emulsion droplets by OH^- ions.[50] With all the available information collected together, it is reasonable to interpret that the negative surface charge of water mostly stems from anisotropic water dipole orientation, and the contribution of surface OH^- ions should be negligible for neutral water.

(ii) Electric field at the water interface. The question of whether the low value for proton transfer is related to the local electric fields at the interface is indeed an important and relevant one. The presence of strong electric fields at the water interface can potentially influence proton transfer rates and mechanisms. However, it's important to note that the behavior of water at interfaces is a complex and multifaceted topic, and the relationship between electric fields, proton transfer, and the water interface is still an area of active research. In our study, we have observed that the proton transfer mechanism in hydronium ions at the water surface occurs rapidly, with a low energy barrier, indicating a relatively small tunneling effect.[42] This observation suggests that local electric fields at the interface may not be inhibiting proton transfer as strongly as previously thought.

However, it's important to note that the behavior of water at interfaces can vary depending on several factors, including temperature, pressure, and the presence of other solutes or ions, which can lead to different observations in different studies. For instance, the discrepancy between our findings and some literature reports, such as the one[51] suggesting the presence of large electrostatics at the interface, may arise from differences in the specific systems, conditions, or methodologies used in those studies. On the other hand, recent experiments[52] and *ab initio* simulations[53] suggest that the probability of dissociating water at the interface is the same as in the bulk. These findings may indeed be valid for their specific experimental conditions or system setup. These conflicting observations emphasize the complexity of the water interface and the potential sensitivity of its behavior to specific conditions and the need for further investigation of water at interfaces.

Understanding the interplay between electric fields, proton transfer, and the water interface is a complex and challenging task. We acknowledge these contrasting findings and suggest that the behavior of water at interfaces may be highly sensitive to specific conditions. The complex nature of water interfaces, which involve various forces such as electrostatics, hydrogen bonding, and van der Waals interactions, makes it essential to consider a range of factors in interpreting experimental and computational results. Besides, NQEs play a crucial role in the proton transfer process and should be considered in the description of the behavior of light atoms, especially protons in water systems. The inclusion of NQEs in simulations enhances the understanding of accurately modeling the behavior of water and H-bonded systems,[31] proton transfer processes under electric fields, ultimately shedding light on the profound influence of electrostatics and quantum effects on water's behavior. Neglecting NQEs could limit the description of proton behavior, particularly in the presence of electrostatic gradients. However, in our study, we chose to focus on classical molecular dynamics simulations using a QM/MM approach. This choice was made due to the computational demands of full quantum calculations, especially over long timescales and for large systems. We acknowledge that NQEs can impact proton behavior, and this is an important aspect that we have not directly addressed in our current work due to the computational challenges involved in large-scale QM/MM simulations with NQEs. We encourage future research efforts to reconcile these differences and provide a more comprehensive understanding of the role of electric fields at the water interface in proton transfer processes. By addressing these complexities and limitations, we can advance our knowledge of water interfaces and their relevance to various scientific contexts.

(iii) Surface propensity of H_3O^+ and OH^-. Nonlinear optical spectroscopic studies of the water surface structure[4,5] indicate the enhancement of hydronium density at the surface. Similar measurements for hydroxide ions show results that can be interpreted in diverse ways,[4,5] from slight enhancement of OH^- at the surface to strong depletion. The spectroscopic methods used in these works such as vibrational sum-frequency generation (VSFG) probe the structure of the water surface typically within a depth of 1–2 molecular layers, depending on the vibrational structure of interest.[54] This probing depth nicely overlaps with the region of H_3O^+ enhancement, as shown by the depth distribution of H_3O^+ ions in Fig. 2. Therefore, the VSFG technique can be very effective to detect the surface accumulated H_3O^+ ions. On the other hand, OH^- ions prefer to reside in the interior region or can be shallowly trapped below the outermost molecular layer (3–4 Å from the surface, Fig. 2). Under this situation, VSFG detection of OH^- species at the surface will not be as effective as that for H_3O^+.

(iv) pH at the water surface. The degree of the enhancement of H_3O^+ density at the air/water interface has been estimated by measuring the acid–base equilibrium of a surface-active pH indicator with an electronic sum-frequency generation method.[6] The study showed that the pH of the water surface is lower than that of the bulk by about 1.7. The observation quantitatively indicates the degree of enhancement of H_3O^+ activity at the water surface. As pointed out in the previous section, however, the hydronium surface population measured by means of surface reactions may be affected by kinetic effects in addition to the static density profile of the ions. If subsurface hydronium species additionally participated in the acid–base reaction at the surface *via* fast PT events, then the measured pH of the water surface may be lower than the pH corresponding to the static population of hydronium ions. That is, the surface activity of hydronium may depend not only on static population but also on transport dynamics.

4. Conclusions

In order to address the current controversies on the surface states of water, we have performed large scale QM/MM-MD simulations on water surface model systems with and without excess hydroniums and hydroxides. Emphasis was put on understanding for the dynamical behaviors of surface-residing hydroniums and hydroxides and their spatial depth distributions, as well as possible origins of surface charge of water. The following conclusions can be drawn from this study.

(i) Hydronium shows strong preference for a water surface with its free energy minima in the topmost surface layer, which confirms the result of previous simulation studies. The surface-residing hydronium ions can migrate to the interior region *via* proton hopping events, which occur fast ($\sim$0.1 ps) with a low energy barrier ($\sim$0.5 kcal mol^{-1}). As a result, the kinetic depth distribution of hydroniums may be wider than their thermodynamic positional depth distribution.

(ii) Hydroxide does not show strong surface preference owing to the difficulty of maintaining the optimal solvated structure with four hydrogen bonds at the surface. A shallow local energy minimum appears for hydroxide right below the top surface layer at 300 K, and this well depth increases at 250 K. The hydroxide migration mechanism mainly involves slow rotational motion with a barrier height of $\sim$2.0 kcal mol^{-1}, with only minor contribution of a proton transfer mechanism.

(iii) Anisotropic dipole orientation at the water surface generates negative surface charges and corresponding interfacial electric field. This voltage of the dipolar surface phase should be responsible for a large portion of surface potentials of neutral water measured in experiments.

(iv) The thickness of the surface phase of water can vary significantly depending on the properties of interest. The acidic surface phase with enhanced hydronium population exists within a depth of $\sim$3 Å from the surface. Due to fast proton transport, however, the kinetic depth of the acidic surface phase can be significantly extended to $\sim$6 Å. The basic surface phase due to shallow trapping of hydroxides exists in the 3–4 Å region below the surface. The dipolar surface phase of pure water with anisotropic water dipole orientation extends to a depth of $\sim$10 Å.

(v) Therefore, the seemingly contradictory observations that the water surface is more acidic than its interior, by nonlinear optical spectroscopic studies,[4–6] and that the water surface is negatively charged, by electrophoretic measurements,[2,3] can be explained by the surface propensity of hydronium ions and the negative surface charges contributed by surface water dipoles as well as asymmetric electron density distribution. These new discoveries will bring the anisotropic dipole orientation of surface water molecules. These new discoveries will bring our understanding of the water surface properties closer to reality.

Author contributions

Investigation, methodology, writing – review & editing: Md Al Mamunur Rashid; reviewing, visualization: Mofizur Rahman; reviewing, validation, visualization: Thamina Acter; conceptualization, supervision, writing – original draft: Nizam Uddin.

Conflicts of interest

The authors declare no competing financial interest.

Acknowledgements

We are grateful to Professor Cheol Ho Choi, Kyungpook National University, for using his laboratory facilities for this study. This research did not receive any specific grant from funding agencies in the public, commercial, or not-for-profit sectors.

References

1 J. K. Beattie, A. M. Djerdjev and G. G. Warr, The surface of neat water is basic, *Faraday Discuss.*, 2009, **141**, 31–39.
2 A. Graciaa, G. Morel, P. Saulner, J. Lachaise and R. S. Schechter, The Zeta-Potential of Gas-Bubbles, *J. Colloid Interface Sci.*, 1995, **172**, 131–136.
3 J. K. Beattie, A. M. Djerdjev and G. G. Warr, The Surface of Neat Water Is Basic, *Faraday Discuss.*, 2009, **141**, 31–39.
4 P. B. Petersen and R. J. Saykally, Is the Liquid Water Surface Basic or Acidic? Macroscopic Vs. Molecular-Scale Investigations, *Chem. Phys. Lett.*, 2008, **458**, 255–261.
5 C. S. Tian, N. Ji, G. A. Waychunas and Y. R. Shen, Interfacial Structures of Acidic and Basic Aqueous Solutions, *J. Am. Chem. Soc.*, 2008, **130**, 13033–13039.
6 S. Yamaguchi, A. Kundu, P. Sen and T. Tahara, Communication: Quantitative Estimate of the Water Surface $_{P}$H Using Heterodyne-Detected Electronic Sum Frequency Generation, *J. Chem. Phys.*, 2012, **137**, 151101.
7 V. Buch, A. Milet, R. Vacha, P. Jungwirth and J. P. Devlin, Water Surface Is Acidic, *Proc. Natl. Acad. Sci. U. S. A.*, 2007, **104**, 7342–7347.
8 R. Vacha, D. Horinek, M. L. Berkowitzc and P. Jungwirth, Hydronium and Hydroxide at the Interface between Water and Hydrophobic Media, *Phys. Chem. Chem. Phys.*, 2008, **10**, 4975–4980.
9 H.-S. Lee and M. E. Tuckerman, Ab Initio Molecular Dynamics Studies of the Liquid-Vapor Interface of an HCl Solution, *J. Phys. Chem. A*, 2009, **113**, 2144–2151.
10 R. Kumar, C. Knight and G. A. Voth, Exploring the Behaviour of the Hydrated Excess Proton at Hydrophobic Interfaces, *Faraday Discuss.*, 2013, **167**, 263–278.
11 J. S. Hub, M. G. Wolf, C. Caleman, P. J. van Maaren, G. Lowerenhoff and D. van der Spoel, Thermodynamics of Hydronium and Hydroxide Surface Solvation, *Chem. Sci.*, 2014, **5**, 1745–1749.
12 L. X. Dang, Solvation of the Hydronium Ion at the Water Liquid Vapor Interface, *J. Chem. Phys.*, 2003, **119**, 6351–6353.

13 C. J. Mundy, I.-F. W. Kuo, M. E. Tuckerman, H.-S. Lee and D. J. Tobias, Hydroxide Anion at the Air–Water Interface, *Chem. Phys. Lett.*, 2009, **481**, 2–8.
14 M. D. Baer, I.-F. W. Kuo, D. J. Tobias and C. J. Mundy, Toward a Unified Picture of the Water Self-Ions at the Air–Water Interface: A Density Functional Theory Perspective, *J. Phys. Chem. B*, 2014, **118**, 8364–8372.
15 C. D. Wick, Hydronium Behavior at the Air–Water Interface with a Polarizable Multistate Empirical Valence Bond Model, *J. Phys. Chem. C*, 2012, **116**, 4026–4038.
16 M. A. Wilson, A. Pohorille and L. R. Pratt, Molecular-Dynamics of the Water Liquid Vapor Interface, *J. Phys. Chem.*, 1987, **91**, 4873–4878.
17 L. X. Dang and T. M. Chang, Molecular Mechanism of Ion Binding to the Liquid/Vapor Interface of Water, *J. Phys. Chem. B*, 2002, **106**, 235–238.
18 S. I. Mamatkulov, P. K. Khabibullaev and R. R. Netz, Water at Hydrophobic Substrates: Curvature, Pressure, and Temperature Effects, *Langmuir*, 2004, **20**, 4756–4763.
19 S. M. Kathmann, I. F. W. Kuo, C. J. Mundy and G. K. Schenter, Understanding the Surface Potential of Water, *J. Phys. Chem. B*, 2011, **115**, 4369–4377.
20 R. Vacha, S. W. Rick, P. Jungwirth, A. G. F. de Beer, H. B. de Aguiar, J. S. Samson and S. Roke, The Orientation and Charge of Water at the Hydrophobic Oil Droplet-Water Interface, *J. Am. Chem. Soc.*, 2011, **133**, 10204–10210.
21 J. R. Cendagorta and T. Ichiye, The Surface Potential of the Water–Vapor Interface from Classical Simulations, *J. Phys. Chem. B*, 2015, **119**, 9114–9122.
22 S. M. Kathmann, I.-F. W. Kuo, C. J. Mundy and G. K. Schenter, Understanding the Surface Potential of Water, *J. Phys. Chem. B*, 2011, **115**, 4369–4377.
23 K. Leung, Surface Potential at the Air-Water Interface Computed Using Density Functional Theory. J. Phys, *Chem. Lett.*, 2010, **1**, 496–499.
24 S. M. Kathmann, I.-F. W. Kuo and C. J. Mundy, Electronic Effects on the Surface Potential at the Vapor-Liquid Interface of Water, *J. Am. Chem. Soc.*, 2008, **130**, 16556–16561.
25 L. X. Dang and T.-M. Chang, Molecular Dynamics Study of Water Clusters, Liquid, and Liquid–Vapor Interface of Water with Many-Body Potentials, *J. Chem. Phys.*, 1997, **106**, 8149–8159.
26 S. E. Feller, R. W. Pastor, A. Rojnuckarin, S. Bogusz and B. R. Brooks, Effect of Electrostatic Force Trunction on Interfacial and Transport Properties of Water, *J. Phys. Chem.*, 1996, **100**, 17011–17020.
27 G. Casseone, Nuclear Quantum Effects Largely Influence Molecular Dissociation and Proton Transfer in Liquid Water under an Electric Field, *J. Phys. Chem. Lett.*, 2020, **11**, 8983–8988.
28 M. Ceriotti, J. Cuny, M. Parrinello and D. E. Manolopoulos, Nuclear quantum effects and hydrogen bond uctuations in water, *Proc. Natl. Acad. Sci. U. S. A.*, 2013, **110**, 15591–15596.
29 O. Marsalek and T. E. Markland, Quantum dynamics and spectroscopy of ab initio liquid water: the interplay of nuclear and electronic quantum effects, *J. Phys. Chem. Lett.*, 2017, **8**, 1545–1551.
30 F. Mouhat, S. Sorella, R. Vuilleumier, A. M. Saitta and M. Casula, Fully quantum description of the Zundel ion: combining variational quantum Monte Carlo with path integral Langevin dynamics, *J. Chem. Theory Comput.*, 2017, **13**, 2400.
31 D. H. Lee, J. Bang and H. Kang, Surface Charge Layer of Amorphous Solid Water with Adsorbed Acid or Base: Asymmetric Depth Distributions of H^+ and OH^- Ions, *J. Phys. Chem. C*, 2016, **120**, 12051–12058.
32 C. H. Choi, S. Re, M. Feig and Y. Sugita, Quantum Mechanical/Effective Fragment Potential Molecular Dynamics (QM/EFP-MD) Study on Intra-Molecular Proton Transfer of Glycine in Water, *Chem. Phys. Lett.*, 2012, **539**, 218–221.
33 N. Uddin, T. H. Choi and C. H. Choi, Origin of Acid–Base Catalytic Effects on Formaldehyde Hydration, *J. Phys. Chem. A*, 2016, **120**, 9598–9606.
34 M. K. Ghosh, T. H. Choi and C. H. Choi, Conformational Free Energy Surfaces of Non-Ionized Glycine in Aqueous Solution, *Theor. Chem. Acc.*, 2016, **135**, 1–11.
35 N. Uddin, M. K. Ghosh, T. H. Choi and C. H. Choi, Gauche Effects of Glucopyranose by QM/MM-MD Simulations, *Theor. Chem. Acc.*, 2015, **134**, 1–10.
36 M. K. Ghosh, T. H. Choi and C. H. Choi, Like-Charge Ion Pairs of Hydronium and Hydroxide in Aqueous Solution?, *Phys. Chem. Chem. Phys.*, 2015, **17**, 16233–16237.
37 N. Uddin, T. H. Choi and C. H. Choi, Direct Absolute pk_a Predictions and Proton Transfer Mechanisms of Small Molecules in Aqueous Solution by QM/MM-MD, *J. Phys. Chem. B*, 2013, **117**, 6269–6275.
38 M. K. Ghosh, S. Re, M. Feig, Y. Sugita and C. H. Choi, Interionic Hydration Structures of NaCl in Aqueous Solution: A Combined Study of Quantum Mechanical Cluster Calculations and QM/EFP-MD Simulations, *J. Phys. Chem. B*, 2013, **117**, 289–295.
39 C. H. Choi, S. Re, M. H. O. Rashid, H. Li, M. Feig and Y. Sugita, Solvent Electronic Polarization Effects on Na^+-Na^+ and Cl^--Cl^- Pair Associations in Aqueous Solution, *J. Phys. Chem. B*, 2013, **117**, 9273–9279.
40 M. K. Ghosh, J. Lee, C. H. Choi and M. Cho, Direct Simulations of Anharmonic Infrared Spectra Using Quantum Mechanical/Effective Fragment Potential Molecular Dynamics (QM/EFP-MD): Methanol in Water, *J. Phys. Chem. A*, 2012, **116**, 8965–8971.
41 M. K. Ghosh, N. Uddin and C. H. Choi, Hydrophobic and Hydrophilic Associations of a Methanol Pair in Aqueous Solution, *J. Phys. Chem. B*, 2012, **116**, 14254–14260.
42 N. Uddin, J. Kim, B. J. Sung, T. H. Choi, C. H. Choi and H. Kang, Comparative Proton Transfer Efficiencies of Hydronium and Hydroxide in Aqueous Solution: Proton Transfer vs Brownian Motion, *J. Phys. Chem. B*, 2014, **118**, 13671–13678.
43 A. Grossfield, Wham: The Weighted Histogram Analysis Method, Version 2.0.9, (**https://Membrane.Urmc.Rochester.Edu/Content/Wham**) 2012.
44 Z. Fangqiang and H. Gerhard, Convergence and error estimation in free energy calculations using the weighted

histogram analysis method, *J. Comput. Chem.*, 2011, **33**, 453–465.

45 M. W. Schmidt, *et al.*, General Atomic and Molecular Electronic Structure System, *J. Comput. Chem.*, 1993, **14**, 1347–1363.

46 D. H. Lee, C. H. Choi, T. H. Choi, B. J. Sung and H. Kang, Asymmetric Transport Mechanisms of Hydronium and Hydroxide Ions in Amorphous Solid Water: Hydroxide Goes Brownian While Hydronium Hops, *J. Phys. Chem. Lett.*, 2014, **5**, 2568–2572.

47 D. T. Sawyer, *Oxygen Chemistry*, Oxford University Press, 1991.

48 J. Thøgersen, S. K. Jensen, C. Petersen and S. R. Keiding, Reorientation of Hydroxide Ions in Water, *Chem. Phys. Lett.*, 2008, **466**, 1–5.

49 R. J. Hunter, *Zeta Potential in Colloid Science*, ed., R. H. Ottewill, R. L. Rowell, Academic Press, New York, 1981.

50 J. K. Beattie and A. M. Djerdjev, The Pristine Oil/Water Interface: Surfactant-Free Hydroxide-Charged Emulsions, *Angew. Chem., Int. Ed.*, 2004, **43**, 3568–3571.

51 M. T. C. Martins-Costa and M. F. R. López, Electrostatics and Chemical Reactivity at the Air–Water Interface, *J. Am. Chem. Soc.*, 2023, **145**, 1400–1406.

52 A. G. Adair Jr., N. H. Musskopf, X. Liu, Z. Yang, J. Petry, P. Zhang, S. Thoroddsen, H. Im and H. Mishra, On the formation of hydrogen peroxide in water microdroplets, *Chem. Sci.*, 2022, **13**, 2574–2583.

53 F. Creazzo, S. Pezzotti, S. Bougueroua, A. Serva, J. Sponer, F. Saija, G. Cassone and M. P. Gaigeot, Enhanced conductivity of water at the electrified air–water interface: a DFT-MD characterization, *Phys. Chem. Chem. Phys.*, 2020, **22**, 10438–10446.

54 T. Ishihara, T. Ishiyama and A. Morita, Surface Structure of Methanol/Water Solutions Via Sum Frequency Orientational Analysis and Molecular Dynamics Simulation, *J. Phys. Chem. C*, 2015, **119**, 9879–9889.